Permanent Magnet Materials

Satoshi Okamoto

Abstract The characterization of permanent magnets is important for industries and academics. Moreover, the magnetic properties of permanent magnets have many aspects from macroscopic and microscopic views. For these different standpoints, we must select proper magnetic measurements and analyses. In this chapter, various magnetic measurements and analyses are concisely explained to help the readers who have different backgrounds.

Keywords Permanent magnet · Nd–Fe–B · Magnetization curve · FORC · Magnetic viscosity · Magnetization reversal process · XMCD

1 Introduction

Permanent magnets have been important materials for motors and generators that convert electricity to power and vice versa. Their importance has increased because of the recent drastic shift of vehicle powertrain from fossil fuel to electricity. Therefore, the demand for high-performance permanent magnets has increased significantly [1–3]. To respond to this demand, how can we characterize permanent magnets? Which measurement method and analysis should be used? From the industrial standpoint, the most important parameter of permanent magnets is the energy product $(BH)_{\max}$, which is defined as the maximum product of magnetic flux density B and magnetic field H. Thus, for this purpose, accurate measurement of the intrinsic magnetization curve of a permanent magnet is critical. On the other hand, the physical origin of coercivity and the magnetization reversal process of permanent magnets are the major concerns for academic researchers. These issues are not only of academic interests but also important to improve the properties of permanent magnets. For these research purposes, time- and temperature-dependent

S. Okamoto (✉)
IMRAM, Tohoku University, Sendai, Japan
e-mail: satoshi.okamoto.c1@tohoku.ac.jp

V. Franco, B. Dodrill (eds.), *Magnetic Measurement Techniques for Materials Characterization*, https://doi.org/10.1007/978-3-030-70443-8_22

magnetization curve measurements and/or high-spatial-resolution magnetic imaging techniques are required.

In this chapter, general notes for the magnetization curve measurements of permanent magnets are explained in Sect. 2. Then, after brief explanations on coercivity and magnetization reversal analyses for permanent magnets, some examples for these analyses are presented in Sects. 3 and 4.

2 General Notes for Magnetization Curve Measurements of Permanent Magnets

Magnetization curves of permanent magnets are measured by various methods, such as dc *B-H* tracer, pulse *B-H* tracer, and vibrating sample magnetometer (VSM) [4]. In a dc *B-H* tracer, a magnet sample is sandwiched by electromagnet poles, making a closed magnetic circuit. Consequently, the intrinsic magnetization curve of the magnet sample can be measured without any demagnetization correction treatments, because the demagnetization field does not exist inside the magnet sample placed in the closed magnetic circuit. This advantage of the dc *B-H* tracer that is attributed to the use of electromagnets becomes a disadvantage for the measurement of very high coercivity magnet samples because of the limitation of the magnetic field of 3 T or less. Moreover, the saturation of the magnetic pole at the high-field region causes a nonlinear signal change because of the mirror effect. On the other hand, a pulse *B-H* tracer can apply a much larger magnetic field; however, this method uses an open magnetic circuit. Therefore, the magnetization curve measured by this method is deformed from its intrinsic curve shape because of the shape-dependent demagnetization field. In addition to the demagnetization field, the application of a large pulse field may further deform the magnetization curve because of the eddy current effect when the magnet sample is metallic. A VSM has a very high sensitivity and is widely used for academic research. However, because a VSM has an open magnetic circuit like a pulse *B-H* tracer, the magnetization curve also deforms due to the demagnetization field.

Usually, a cuboid sample is used for the magnetization curve measurements because of easy sample shaping and easy sample mounting on the sample holder of the measurement apparatus. However, the demagnetization factor inside the cuboid sample is not uniform, making the demagnetization field correction difficult. Some textbooks state that a spheroid sample is effective for the demagnetization field correction because of the uniform demagnetization field inside the body. This, however, is valid only when the sample is uniformly magnetized, that is, in the fully saturated state. When permanent magnets are demagnetized, this assumption is not valid. During the demagnetization process of permanent magnets, large magnetic domains are observed in Nd–Fe–B sintered magnets [5]. Thus, the demagnetization field becomes nonuniform during the demagnetization process even for the spheroid samples. For anisotropic permanent magnets, a pillar-shaped

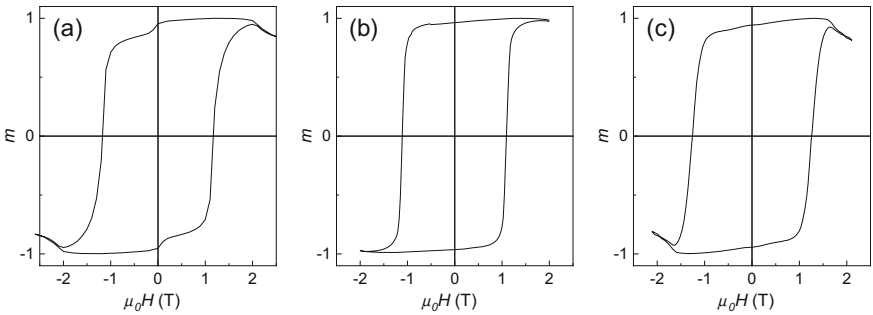

Fig. 1 Magnetization curves of pillar-shaped (**a**) Nd–Fe–B sintered, (**b**) Nd–Fe–B hot-deformed, and Sm_2Co_{17} magnets. (**a**) and (**b**) are measured at RT, and (**c**) is measured at 200 °C

sample that has the long axis along the magnetic easy axis can minimize this difficulty of demagnetization correction [6].

Finally, the surface-damaged layer of permanent magnets should be mentioned. Figure 1 shows the magnetization curves of pillar-shaped Nd–Fe–B sintered, Nd–Fe–B hot-deformed, and Sm_2Co_{17} magnets measured by VSM. The nonlinear decrease in magnetization in the high-field region is attributed to the mirror effect. For the Nd–Fe–B sintered magnet shown in Fig. 1(a), a kink on the magnetization curve at around zero magnetic field is obviously found, indicating the presence of the magnetic soft phase of the surface-damaged layer [7]. This surface-damaged layer is due to the mechanical polishing process of sample shaping. The thickness of the surface-damaged layer of Nd–Fe–B sintered magnets is estimated to be several tens of micrometers [4], corresponding to a thickness of approximately several grains. This surface-damaged layer thickness strongly depends on the permanent magnet material and its microstructure. In fact, Nd–Fe–B hot-deformed and Sm_2Co_{17} magnets, shown in Fig. 1(b, c), do not exhibit the kink at around zero magnetic field on their magnetization curves, indicating that the surface-damaged layer is negligibly thin in these magnets.

3 Coercivity Analysis of Permanent Magnets

Generally, the coercivity of permanent magnets is small compared with the anisotropy field, which is the theoretical upper limit of coercivity [8, 9]. This is called as “Brown’s paradox” [10]. Because the coercivity is a very important parameter of permanent magnets, the coercivity mechanism has long been studied to solve Brown’s paradox. The magnetization reversal process of permanent magnets is roughly categorized into two types, the nucleation and wall pinning types, as illustrated in Fig. 2(a, b), respectively. The former proceeds via avalanche-like domain wall propagation initiated by a nucleation of a small reversed domain. The

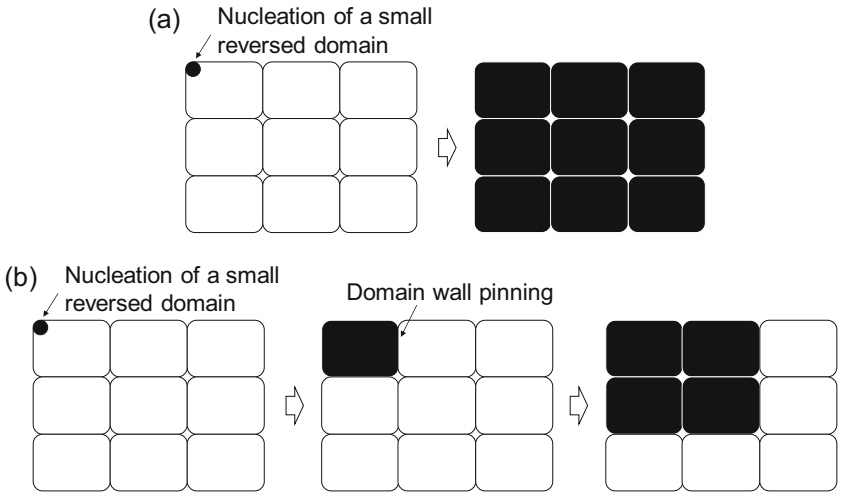

Fig. 2 Illustrations of magnetization reversal processes of (**a**) nucleation and (**b**) domain wall pinning

latter is also initiated by a nucleation of a small reversed domain. However, the domain does not expand until a certain critical field due to the domain wall pinning.

Two different approaches for these issues have been studied so far. One is the static analysis developed by Kromüller [8, 9]. The other is the thermal activation analysis by Givord [11–13]. In the following subsections, these models and examples of analyzed results are briefly explained.

Static Analysis

Kromüller assumed a one-dimensional model of a very thin soft magnetic layer sandwiched by a hard magnetic phase that mimics a defect layer or a grain boundary. He calculated the coercivity H_c for nucleation and/or pinning cases based on the one-dimensional micromagnetics theory [8, 9]. Consequently, he deduced the following simple equation:

$$H_c = \alpha H_k - N_{eff} M_s, \tag{1}$$

where H_k is the anisotropy field, M_s is the saturation magnetization, α is the reduction coefficient related to the soft-region magnetic anisotropy and/or easy axis orientation, and N_{eff} is the effective local demagnetization coefficient. Kromüller elaborately studied the form of α for various cases of nucleation/pinning, and as a result, he derived that α is given as a function of r_0/δ_B, where r_0 is the thickness of

the soft magnetic phase and δ_B is the domain wall thickness of the hard magnetic phase. This equation has been widely accepted for many experimental researchers to analyze the coercivity empirically, and the values of α and N_{eff} have been evaluated from the plot of temperature-dependent H_c/M_s vs. H_k/M_s. Usually, the value of H_k in this analysis is treated as the literature data. Thus, the obtained α and N_{eff} are regarded as temperature-independent empirical parameters. However, as mentioned above, α is a temperature-dependent parameter, because α is the function of r_0/δ_B. Therefore, the naive empirical adoption of Eq. (1) may lead to values of α and N_{eff} that are quite different from the ones originally considered by Kromüller.

Thermal Activation Analysis

Kromüller's theory does not consider the thermal activation effect on the magnetization reversal. One might say that the thermal activation effect does not need to be considered for permanent magnets, because permanent magnets are bulk materials. However, the actual magnetization reversal is triggered by the nucleation of a very small reversed domain with nanometer scale. In this size range, thermal activation becomes crucial. In fact, when a permanent magnet is kept in a constant reverse magnetic field, the magnetization logarithmically decreases with time because of the thermal activation effect. This behavior is known as magnetic viscosity [14]. The time-dependent magnetization $M(t)$ in the magnetic viscosity is expressed as.

$$M(t) = M(0) - S \ln t, \tag{2}$$

where S is the magnetic viscosity coefficient. Wohlfarth [15] and Gaunt [16] developed the theory of the magnetic viscosity and derived the following relation:

$$S = -k_B T \chi_{irr} / \left(\frac{dE}{dH} \right), \tag{3}$$

where χ_{irr} is the irreversible magnetic susceptibility, $k_B T$ is the thermal energy, H is the applied field, and E is the energy barrier for the magnetization reversal. Generally, E is a function of H given as.

$$E(H) = E_0(1 - H/H_0)^n, \tag{4}$$

where E_0 is the barrier height at $H = 0$, H_0 is the critical field for the magnetization reversal without thermal activation effect, and n is a constant depending on the magnetization reversal process, i.e., $n = 2$ for coherent rotation [17] and $n = 1$ for a weak pinning case [16]. Thus, by substituting Eq. (4) into Eq. (3), we get the relation of

$$S/\chi_{\mathrm{irr}} \,(\equiv H_{\mathrm{f}}) = k_{\mathrm{B}}T/\left[n\frac{E_0}{H_0}\left(1-\frac{H}{H_0}\right)^{n-1}\right] \tag{5}$$

Thus, the defined H_{f} is called as the fluctuation field, and is obtained from the separately measured values of S and χ_{irr}. H_{f} can be also obtained only from the magnetic viscosity measurements as [18]

$$H_{\mathrm{f}}(H) = \frac{\Delta H}{\Delta \ln (S/t)}. \tag{6}$$

Givord et al. found that the values of S and χ_{irr} of Nd–Fe–B sintered magnets exhibited the same trends against H [11], indicating that H_{f} is a constant irrespective of H. This fact leads to $n = 1$ in Eqs. (4) and (5). Considering the normal measurement condition of coercivity using VSM, that is, several seconds of data acquisition time for each data point, E corresponds to $25k_{\mathrm{B}}T$. Moreover, assuming the effective magnetization reversal field $H = H_{\mathrm{c}} + N_{\mathrm{eff}}M_{\mathrm{s}}$, Eq. (4) with $n = 1$ is transformed into.

$$H_{\mathrm{c}} = \frac{E_0}{M_{\mathrm{s}}v_{\mathrm{act}}} - N_{\mathrm{eff}}M_{\mathrm{s}} - 25H_{\mathrm{f}}, \tag{7}$$

where $v_{\mathrm{act}} = k_{\mathrm{B}}T/M_{\mathrm{s}}H_{\mathrm{f}}$ is the activation volume. Consequently, the follow equation is given by assuming $E_0 = \alpha\gamma_{\mathrm{w}}{v_{\mathrm{act}}}^{2/3}$ [12]:

$$H_{\mathrm{c}} = \alpha\frac{\gamma_{\mathrm{w}}}{M_{\mathrm{s}}{v_{\mathrm{act}}}^{1/3}} - N_{\mathrm{eff}}M_{\mathrm{s}} - 25H_{\mathrm{f}}, \tag{8}$$

where γ_{w} is the domain wall energy. Obviously, Eq. (8) derived from the thermal activation model has the similar form of Eq. (1) proposed by Kromüller.

Note that Eqs. (7) and (8) are only valid for $n = 1$ in Eq. (4). Very recently, Okamoto et al. proposed a more general thermal activation analysis for permanent magnets based on the magnetic viscosity measurements [19]. Magnetic viscosity measurements starting from various magnetic fields just above H_{c} also give the time-dependent coercivity $H_{\mathrm{c}}(t)$, with an example shown in Fig. 3. $H_{\mathrm{c}}(t)$ for the magnet with the energy barrier of Eq. (4) was formulated by Sharrock [20] as.

$$H_{\mathrm{c}}(t) = H_0\left[1-\left\{\frac{k_{\mathrm{B}}T}{E_0}\ln\left(\frac{f_{\mathrm{o}}t}{\ln 2}\right)\right\}^{1/n}\right], \tag{9}$$

where f_0 is the attempt frequency with the order of 10^9–10^{11} Hz. Here, there are three unknown parameters (H_0, E_0, and n), and these cannot be determined simultaneously only from the experimentally values of $H_{\mathrm{c}}(t)$. However, these three parameters are determined from the analysis by combining $H_{\mathrm{c}}(t)$ and H_{f} [19]. Figure 4 shows examples of the thus obtained values of H_0, E_0, and n of Nd–Fe–B hot-deformed magnets. HD and GBD denote the differently processed magnets

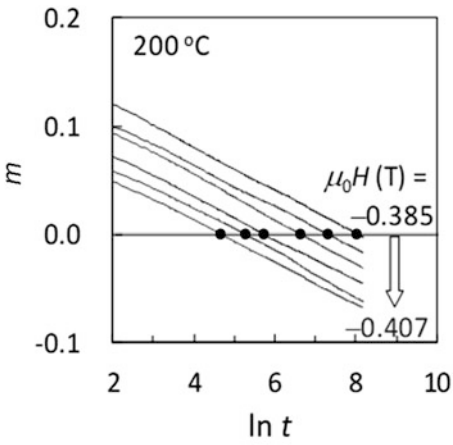

Fig. 3 Example of magnetic viscosity curves of a hot-deformed Nd–Fe–B magnet measured at 200 °C. The intersection with the line of $m = 0$ give the time-dependent coercivity $H_c(t)$

with quite different $\mu_0 H_c$ of 1.1 and 2.2 T, respectively, at ambient temperature. Moreover, these values of $\mu_0 H_c$ decrease significantly with temperature. The values of $\mu_0 H_0$ are well consistent with these very different values of $\mu_0 H_c$ of HD and GBD magnets and their large temperature dependences. On the other hand, the values of n are almost 1 irrespective of magnets and temperature. The values of E_0 is also less dependent on magnets and temperature. These experimental results reflect the feature of the magnetization reversal process of Nd–Fe–B hot-deformed magnets, as discussed in the next section.

4 Magnetization Reversal Process of Permanent Magnets

Magnetic Imaging

Direct observation techniques of the magnetization reversal process of permanent magnets are magnetic imaging, such as magneto-optical Kerr (MOKE) and X-ray magnetic circular dichroism (XMCD) microscopies.

MOKE microscopy utilizes the change of optical polarization of the reflected light from the magnet surface. Therefore, the polished mirror surface is indispensable. This means that the MOKE signal reflects the magnetization state of the polished surface of the magnets. In fact, the coercivity obtained from the MOKE measurement is much smaller than that of the magnet measured by VSM [21], indicating that the polished surface layer loses the hard magnetic property due to the mechanical damage. Nevertheless, it is conceivable that the magnetic domain image by the MOKE microscopy reflects, to some extent, the magnetization state underneath the surface-damaged layer because of the strong magneto-static interaction. Figure 5 shows examples of MOKE images of a Nd–Fe–B sintered magnet. The domain wall displacements inside the grains are clearly observed.

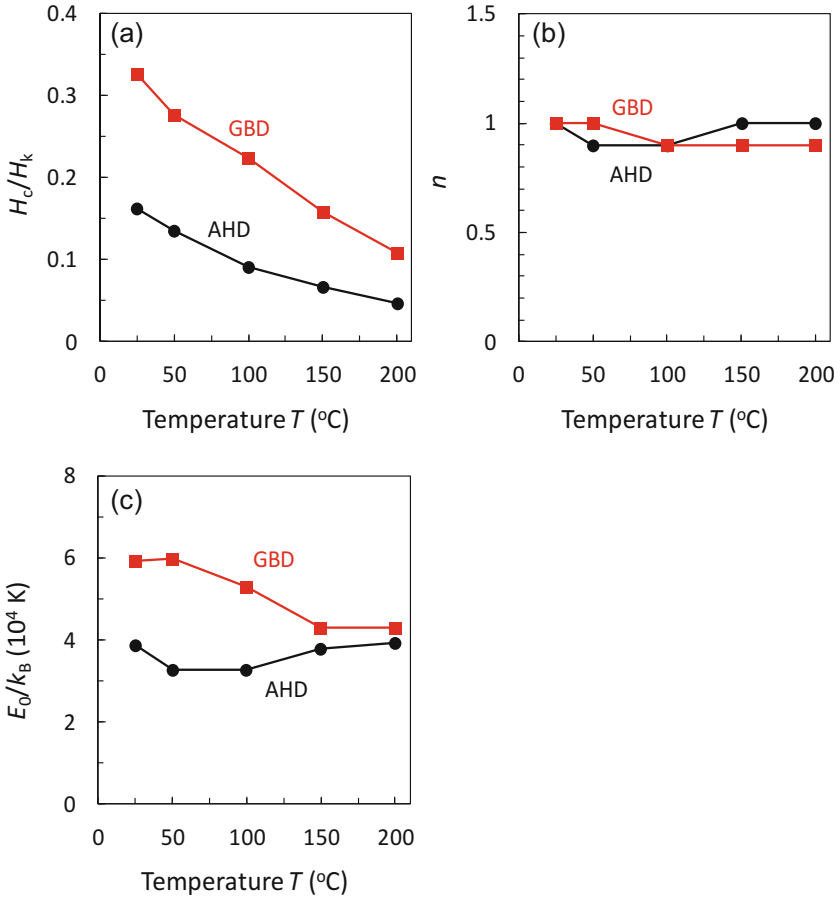

Fig. 4 Energy barrier parameters obtained of a hot-deformed Nd–Fe–B magnets from of thermal activation analysis. (**a**) H_0, (**b**) n, (**c**) E_0 are the parameters of Eq. (4). GBD and HD denote the differently processed magnets with different coercivities

XMCD microscopy is available at synchrotron radiation facilities. Unlike MOKE microscopy, XMCD microscopy does not need the mirror polished surface, because the XMCD signal is obtained from the difference in the X-ray absorption for different helicities. Very recently, Nakamura et al. established the sample fracturing technique inside the XMCD microscopy chamber, which is in ultrahigh vacuum atmosphere [22]. Because Nd–Fe–B sintered magnets favor to fracture at the thin Nd-rich grain boundary phase rather than the $Nd_2Fe_{14}B$ main phase grains, this technique makes it possible to observe the very fresh and non-damaged Nd–Fe–B magnet surface covered with the thin Nd-rich grain boundary phase. Using this technique, they successfully demonstrated that the magnetization curve of a Nd–Fe–B sintered magnet obtained by XMCD agrees very well with that by VSM,

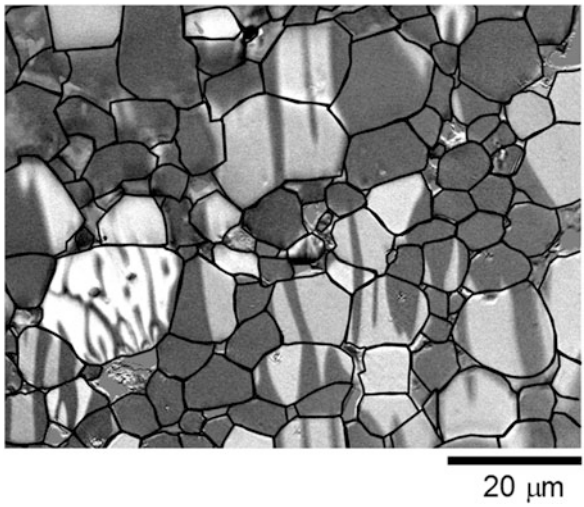

Fig. 5 Example of a MOKE image of a Nd–Fe–B sintered magnet

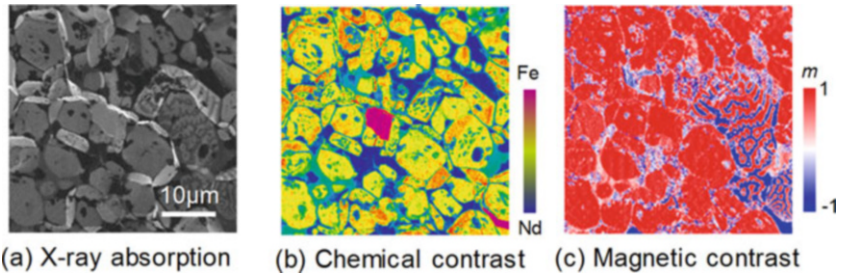

Fig. 6 Examples of multiple images of a Nd–Fe–B sintered magnet using a MOKE microscopy. (**a**) X-ray absorption, (**b**) chemical contrast of Fe and Nd, (**c**) magnetic contrast images. Experiment was performed at BL25SU of SPring-8

indicating that the magnetization state of the fractured surface is almost identical to that of the bulk inside. Moreover, XMCD microscopy makes it possible to obtain multiple images of topographic, chemical, and magnetic contrast, as in the examples shown in Fig. 6. Since Nd–Fe–B sintered magnets consist of various phases other than the $Nd_2Fe_{14}B$ main phase, such as the metallic Nd-rich phase and oxidized Nd as triple junction and grain boundary phases, this multiple imaging of XMCD microscopy is very powerful to reveal the relation of the magnetization reversal process with the microstructure [23].

FORC Analysis

As explained in the preceding section, magnetic imaging is the direct method to visualize the magnetization reversal process of permanent magnets; however, the

information is limited to the surfaces of the magnets. In contrast, first-order reversal curve (FORC) analysis is regarded as a method to visualize the magnetization reversal process of bulk magnets, even though it is not in a direct way. In this sense, magnetic imaging and FORC analysis are complementary. Originally, FORC analysis was established to evaluate the coercivity and interaction field dispersions based on the Preisach model [24] (please see Sect. 3.1). The Preisach model assumes a magnet consisting of a large number of hysteresis units known as hysterons. This assumption, however, is inappropriate for many permanent magnets, especially for Nd–Fe–B magnets. As seen in Figs. 5 and 6, because many multi-domain grains are observed in the Nd–Fe–B sintered magnets, the magnetization reversal in Nd–Fe–B sintered magnets cannot be described by the simple assembly of hysterons. In the FORC measurement, many reversal magnetization curves that start from H_r on the demagnetization curve are recorded with H, and then, the magnetization m on each reversal curve is given as a function of H_r and H. The FORC distribution ρ is defined as a second-order derivative of m with respect to H and H_r:

$$\rho\left(H, H_r\right) = -\frac{\partial}{\partial H_r}\left(\frac{\partial m}{\partial H}\right). \tag{10}$$

This equation represents the variation of magnetic susceptibility ($\partial m/\partial H$) on H_r, corresponding to the irreversible change in the magnetic susceptibility. Thus, the FORC diagram of permanent magnets can be regarded as the contour map of the irreversible magnetization reversal on the (H, H_r) plane rather than the understanding based on the Preisach model.

Figure 7 shows the FORC diagrams of pillar-shaped Nd–Fe–B sintered [25], Nd–Fe–B hot-deformed [26], and Sm_2Co_{17} magnets [27]. These magnet samples are the same as shown in Fig. 1. The magnetization curves of these magnets shown in Fig. 1 are similar rectangles; however, their FORC diagram patterns are quite different. The FORC diagram pattern of the Nd–Fe–B sintered magnet exhibits two spots at around the low-field and high-field regions, indicating that there are two regions of irreversible magnetization reversals. The high-field spot is easily assigned to the magnetization reversal at around the coercivity. On the other hand, the low-field spot evidences that the nontrivial amount of magnetization reversal occurs at very low-field region in the Nd–Fe–B sintered magnet. This low-field spot has been widely observed in various Nd–Fe–B sintered magnets [28]. According to the recent study on the XMCD microscopy observation under the field sequence for the low-field spot of the FORC diagram, the magnetization reversal for the low-field spot is assigned to the domain wall displacement inside the multi-domain grains [25]. In contrast, the FORC diagrams of the Nd–Fe–B hot-deformed and the Sm_2Co_{17} magnets exhibit the high-field spot only, which corresponds to the magnetization reversal at around the coercivity. These different FORC diagrams clearly reflect the different magnetization reversal process of these magnets. Whereas there are multi-domain grains in Nd–Fe–B sintered magnets in which the domain wall smoothly moves, the domain walls in Nd–Fe–B hot-deformed and the Sm_2Co_{17} magnets cannot move smoothly in the low-field region because of the very high density

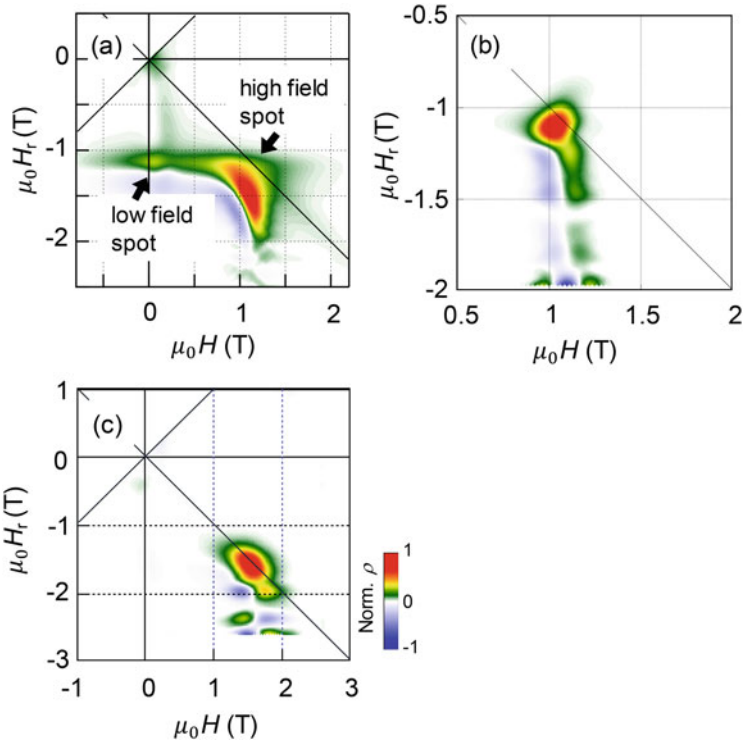

Fig. 7 FORC diagrams of pillar-shaped (**a**) Nd–Fe–B sintered, (**b**) Nd-Fe-B hot-deformed, and (**c**) Sm_2Co_{17} magnets. Samples are the same shown in Fig. 1. (**a**) and (**b**) are measured at RT, and (**c**) is measured at 200 °C

of pinning sites in these magnets. Consequently, the low-field spot in the FORC diagram of these two magnets disappears. Moreover, the positions of these high- and low-field spots and their width give more detailed information on the magnetization reversal process of permanent magnets [29].

5 Summary

Although the study on permanent magnets has very long history, there are still many issues to be studied. Recently, multilateral analyses become very important. The magnetic measurements and analyses explained in this chapter are one approach of them. Moreover, recent advancements of electron microscopy, computer science, synchrotron radiation, and so on are very dramatic. By combining with these cutting-edge technologies, it is highly expected that the magnetic measurements and analyses for permanent magnets will move into new stages. As explained in

Sect. 4.2, FORC analysis combined with XMCD microscopy is one example. This kind of evolution will not only deepen our understandings but also open new fields of studies on permanent magnets.

References

1. J.M.D. Coey, Hard magnetic materials: A perspective. IEEE Trans. Magn. **47**, 4671–4681 (2011). https://doi.org/10.1109/TMAG.2011.2166975
2. S. Sugimoto, Current status and recent topics of rare-earth permanent magnets. J. Phys. D. Appl. Phys. **44**, 064001 (2011). https://doi.org/10.1088/0022-3727/44/6/064001
3. S. Hirosawa, Current status of research and development toward permanent magnets free from critical elements. J. Magn. Soc. Jpn. **39**, 85–95 (2015). https://doi.org/10.3379/msjmag.1504R004
4. Yamamoto H (2019) Basics of permanent magnet and its magnetic measurement. NEODI-CONSUL (in Japanese)
5. J.D. Livingston, Magnetic domains in sintered Fe-Nd-B magnets. J. Appl. Phys. **57**, 4137–4139 (1985). https://doi.org/10.1063/1.334644
6. T. Yomogita et al., First-order reversal curve analysis in hot-deformed Nd–Fe–B magnets, in *Proc. 24th Inter. Workshop on Rare-Earth and Future Permanent Magnets and Their Applications (REPM)*, vol. 2016, (2016), pp. 649–653
7. T. Fukagawa, S. Hirosawa, Coercivity generation of surface $Nd_2Fe_{14}B$ grains and mechanism of fcc-phase formation at the Nd/$Nd_2Fe_{14}B$ interface in Nd-sputtered Nd–Fe–B sintered magnets. J. Appl. Phys. **104**, 013911 (2008). https://doi.org/10.1063/1.2952556
8. H. Kronmüller, Theory of nucleation fields in inhomogeneous ferromagnets. Phys. Stat. Sol. (b) **144**, 385–396 (1987). https://doi.org/10.1002/pssb.2221440134
9. H. Kronmüller, H.-D. Durst, Analysis of the magnetic hardening mechanism in RE-FeB permanent magnets. J. Magn. Magn. Mater. **74**, 291–302 (1988). https://doi.org/10.1016/0304-8853(88)90202-8
10. W.F. Brown, Virtues and weaknesses of the domain concept. Rev. Mod. Phys. **17**, 15–19 (1945). https://doi.org/10.1103/RevModPhys.17.159
11. D. Givord et al., Magnetic viscosity in different NdFeB magnets. J. Appl. Phys. **61**, 3454 (1987). https://doi.org/10.1063/1.338751
12. D. Givord et al., Experimental approach to coercivity analysis in hard magnetic materials. J. Magn. Magn. Mater. **83**, 183–188 (1990). https://doi.org/10.1016/0304-8853(90)90479-A
13. D. Givord, The physics of coercivity. J. Magn. Magn. Mater. **258–259**, 1–5 (2003). https://doi.org/10.1016/S0304-8853(02)00988-5
14. R. Street, J.C. Woolley, A study of magnetic viscosity. Proc. Phys. Soc. A **62**, 562–572 (1949)
15. E.P. Wohlfarth, The coefficient of magnetic viscosity. J. Phys. F **14**, L155–L159 (1984)
16. P. Gaunt, Magnetic viscosity and thermal activation energy. J. Appl. Phys. **59**, 4129–4132 (1986). https://doi.org/10.1063/1.336671
17. E.C. Stoner, E.P. Wohlfarth, A mechanism of magnetic hysteresis in heterogeneous alloys. Philos. Trans. R. Soc. Lond. Ser. A **240**, 599–642 (1948). https://doi.org/10.1098/rsta.1948.0007
18. M. El-Hilo et al., Fluctuation fields and reversal mechanisms in granular magnetic systems. J. Magn. Magn. Mater. **248**, 360–373 (2002). https://doi.org/10.1016/S0304-8853(02)00146-4
19. S. Okamoto, Temperature-dependent magnetization reversal process and coercivity mechanism in Nd–Fe–B hot-deformed magnets. J. Appl. Phys. **118**, 223903 (2015). https://doi.org/10.1063/1.4937274
20. M.P. Sharrock, Time dependence of switching fields in magnetic recording media. J. Appl. Phys. **76**, 6413–6418 (1994). https://doi.org/10.1063/1.358282

21. M. Takezawa, Analysis of the demagnetization process of Nd–Fe–B sintered magnets at elevated temperatures by magnetic domain observation using a Kerr microscope. J. Appl. Phys. **115**, 17A733 (2014). https://doi.org/10.1063/1.4866894
22. Okamoto S unpublished data
23. T. Nakamura et al., Direct observation of ferromagnetism in grain boundary phase of Nd–Fe–B sintered magnet using soft x-ray magnetic circular dichroism. Appl. Phys. Lett. **105**, 202404 (2014). https://doi.org/10.1063/1.4902329
24. D. Billington et al., Unmasking the interior magnetic domain structure and evolution in Nd–Fe–B sintered magnets through high-field magnetic imaging of the fractured surface. Phys. Rev. Mater. **2**, 104413 (2018). https://doi.org/10.1103/PhysRevMaterials.2.104413
25. I.D. Mayergoyz, Mathematical models of hysteresis. IEEE Trans. Magn. **MAG-22**, 603–608 (1986). https://doi.org/10.1109/TMAG.1986.1064347
26. K. Miyazawa et al., First-order reversal curve analysis of a Nd–Fe–B sintered magnet with soft X-ray magnetic circular dichroism microscopy. Acta Mater. **162**, 1–9 (2019). https://doi.org/10.1016/j.actamat.2018.09.053
27. T. Yomogita et al., Temperature and field direction dependences of first-order reversal curve (FORC) diagrams of hot-deformed Nd–Fe–B magnets. J. Magn. Magn. Mater. **447**, 110–115 (2018). https://doi.org/10.1016/j.jmmm.2017.09.072
28. T. Schrefl et al., First order reversal curve studies of permanent magnets. J. Appl. Phys. **111**, 07A728 (2012). https://doi.org/10.1063/1.3678434
29. S. Okamoto et al., Temperature dependent magnetization reversal process of a Ga-doped Nd–Fe–B sintered magnet based on first-order reversal curve analysis. Acta Mater. **178**, 90–98 (2019). https://doi.org/10.1016/j.actamat.2019.08.004